MICA: A multi-omics method to predict gene regulatory networks in early human embryos

Gregorio Alanis-Lobato[1,*], Thomas E. Bartlett[2,*], Qiulin Huang[1,3*], Claire Simon[1], Afshan McCarthy[1], Kay Elder[4], Phil Snell[4], Leila Christie[4] & Kathy K. Niakan[1,3,5,6]

1 Human Embryo and Stem Cell Laboratory, The Francis Crick Institute, London, UK.
2 Department of Statistical Science, University College, London WC1E 7HB, UK.
3 The Centre for Trophoblast Research, Department of Physiology, Development and Neuroscience, University of Cambridge, Cambridge CB2 3EG, UK.
4 Bourn Hall Clinic, Bourn, Cambridge, CB23 2TN.
5 Wellcome – Medical Research Council Cambridge Stem Cell Institute, University of Cambridge, Jeffrey Cheah Biomedical Centre, Puddicombe Way, Cambridge CB2 0AW, UK
6 Epigenetics Programme, Babraham Institute, Cambridge CB22 3AT, UK
*Equal contribution
Corresponding authors: kkn21@cam.ac.uk; g.alanis.lobato@gmail.com; thomas.bartlett.10@ucl.ac.uk

Abstract

Recent advances in single-cell -omics have been transformative to characterise cell types in challenging to study biological contexts. It is technically difficult to infer transcription factor-gene regulatory interactions from these datasets, especially in contexts with limited single-cell sample number such as the early human embryo. Here we systematically assessed the application of four different linear or non-linear gene regulatory network (GRN) prediction strategies to single-cell simulated and human embryo transcriptome datasets. We also compared how gene expression normalisation methods impact on regulatory network predictions, finding that TPM (transcripts per million reads) outperformed alternative methods. We identified more reproducible GRN inferences using a non-linear method based on mutual information (MI) applied to single-cell transcriptome datasets refined with chromatin accessibility (CA) (called MICA), compared to alternative network prediction methods tested. MICA captures complex non-monotonic dependencies and feedback loops. Using MICA, we generated the first GRN inferences in early human development. MICA predicted co-localisation of the AP-1 transcription factor subunit proto-oncogene JUND and the TFAP2C transcription factor AP-2γ in human preimplantation embryos. These interactions were supported by previous findings in other developmental and stem cell contexts. Overall, our comparative analysis of gene regulatory network prediction methods defines a pipeline that can be applied to single-cell multi-omics datasets in especially challenging contexts to infer interactions between transcription factor expression and target gene regulation.

Introduction

Following the fusion of the oocyte and sperm, the zygote undergoes a series of cell divisions until it forms a blastocyst prior to implantation into the uterus. A human blastocyst is formed of a fluid-filled cavity and approximately 200 cells that comprise three distinct cell types: the trophectoderm (TE), which gives rise to fetal components of the placenta; the primitive endoderm (PE), which forms the yolk sac; and the pluripotent epiblast (EPI), which gives rise to the embryo proper (Blakeley et al., 2015). The specification of these three lineages represents the earliest cell-fate decisions in humans. Understanding the molecular mechanisms that regulate these decisions is important for applications including stem cell biology, regenerative medicine, and reproductive technologies (Niakan et al., 2012).

We do not yet understand how cell fate specification is regulated in the human embryo. Transcription factor (TF) and target gene regulatory interactions associated with cell fate specification in this context would be informative and has not been elucidated. Defining the gene regulatory networks (GRNs) associated with a given cell type at a distinct time in development facilitates characterisation of cell type identity and prediction of the transcriptional regulators and cis-regulatory DNA sequences that may underlie cell fate specification (Davidson and Erwin, 2006; Materna and Davidson, 2007; Peter and Davidson, 2011). Challenges to determining GRNs in early embryos include the small number of cells that contribute to the distinct cell lineages of the human embryo at these early stages of development. Moreover, while single cell -omics technologies facilitate the characterisation of genome-wide gene expression and chromatin accessibility changes in human blastocysts (Blakeley et al., 2015; Li et al., 2018; Liu et al., 2019; Petropoulos et al., 2016; Yan et al., 2013), it is unclear if resolution at this level would allow for accurate predictions of GRNs contributing to cell type specific identity.

The most common computational approach to infer TF-gene regulatory interactions is to model the expression of each target gene as either a linear or non-linear combination of the expression of a set of potential regulators (e.g., the TFs in the dataset of interest) (Dobra et al., 2004; Marbach et al., 2012). The 'target gene' method uses advanced regression methods, such as sparse penalised regression or random forests, to model the expression level of a particular 'target' gene (the response), conditional on the expression levels of a set of other genes (predictors, such as TFs) (Haury et al., 2012; Huynh-Thu et al., 2010). By combining these local network model fits genome-wide, with each gene taking a turn as the response or 'target gene' (Dobra et al., 2004), the GRN is constructed. The linear regression model has previously been used in combination with chromatin accessibility to infer GRNs in human brain organoids (Fleck et al., 2022). Bayesian networks also model the expression of each gene conditional on a set of regulating genes (i.e., parents in the network) by computing how likely it is that each TF in the dataset was responsible for the expression of a certain gene (Kamimoto et al., 2020; Marbach et al., 2012; Pe'er, 2005; Tipping, 2001). The Bayesian/Bagging Ridge model in combination with chromatin accessibility has been used effectively to predict the consequence of gene perturbations and to understand cell fate transitions in the context of development and cellular reprogramming (Argelaguet et al., 2022; Kamimoto et al., 2023). Of note, when fitting Bayesian models it is usually necessary to assume global compatibility (of the local network models), which in turn typically requires that the graph contains no loops (acyclicity). This an assumption which is challenging for biological systems, where feedback loops are a persistent feature (Brandman and Meyer, 2008). In another important group of methods, TF-gene (or more generally gene-gene) interactions are ranked based on a pairwise similarity measure of their expression across cell samples, such as a variant of correlation or mutual information (Daub et al., 2004; Krishnaswamy et al., 2014). Again, alternatives are available that consider conditional statistics (e.g., partial correlation or partial information decomposition) (Chan et al., 2017). Finally, a range of 'black-box' machine learning methods are available that model the expression of each gene in hard to visualise ways using for

example sophisticated non-linear combinations of TF expression values (Shu et al., 2021; Wang et al., 2020).

Although GRN inference methods have been comprehensively compared and developed for whole-tissue or bulk transcriptome analysis (Cahan et al., 2014; Chai et al., 2014; Marbach et al., 2012; Morris et al., 2014; Thompson et al., 2015), the interest in cell type-specific regulatory networks has prompted the application of these methods to single cell RNA-seq (scRNA-seq) datasets (Aibar et al., 2017; Chen and Mar, 2018; Fiers et al., 2018; Iacono et al., 2019; Kang et al., 2021; Mochida et al., 2018; Nguyen et al., 2021; Pratapa et al., 2020; Stone et al., 2021). These previous studies showed that the approaches with the best overall performance belong to the regression and mutual information categories and highlighted the challenges of performing GRN inference on single cell datasets. This is attributed mainly to the heterogeneous and stochastic nature of gene expression in individual cells (Nguyen et al., 2021). Of note is that even state-of-the-art methods that have been evaluated on well-defined benchmark datasets predict a considerable number of false positive interactions (Kang et al., 2021; Marbach et al., 2012; Nguyen et al., 2021; Pratapa et al., 2020; Stone et al., 2021). Most of these false predictions originate from indirect associations, for example a path $a \rightarrow b \rightarrow c$ can result in the prediction of $a \rightarrow c$ even if there is no direct link between those nodes (i.e., a 'transitive edge' in the network). Several methods to eliminate such effects have been proposed (Barzel and Barabási, 2013; Chan et al., 2017; Feizi et al., 2013; Margolin et al., 2006; Wang et al., 2018) but they can be computationally demanding and sensitive to the choice of hyper-parameters (Feizi et al., 2013).

Given the stage of development of human preimplantation embryos and their precious nature, together with the restrictions on such research in some countries, the -omics datasets from human blastocysts are very small compared to those from other biological contexts. This makes it challenging to mine these datasets using GRN inference methods, which require a sufficiently large number of cells to produce reproducible results (Kang et al., 2021; Pratapa et al., 2020). This tight restriction on sample sizes places corresponding restrictions on statistical power, and means that the optimal statistical network inference methodology may be specific to this context. Here, we assessed whether the integration of other types of -omics datasets with transcriptomic-based predictions could help to reduce indirect TF-gene relationships and thereby produce more reliable gene regulatory networks in this setting, especially with restricted sample sizes. We utilised a low number of cell samples in high quality -omics data from early human embryos at the blastocyst stage (6-7 days post-fertilisation) (Blakeley et al., 2015; Petropoulos et al., 2016; Yan et al., 2013) to evaluate the plausibility of our predictions: this has the advantage of being a biological context with only three well-defined cell types to evaluate the plausibility of our predictions.

The aims of this work were (i) to evaluate whether it is possible to infer reliable cell type-specific regulatory networks for each one of the cell types in the early human embryo in spite of the size of the available -omics data, (ii) to determine if the integration of chromatin accessibility data with transcriptome analysis would better inform predictions of GRNs, and (iii) to predict and validate previously unidentified gene regulations in the human blastocyst. Overall, we demonstrate that the available single cell transcriptomic data was most robustly analysed by a non-linear mutual information-based inference method which had been refined with chromatin accessibility data (MICA). The resulting analysis predicted the first GRN in human preimplantation development and showed that the interactions were consistent with the transcripts and proteins that are known to be enriched in specific lineages. MICA predicted a novel putative regulatory interaction between the TFAP2C transcription factor AP-2γ and the AP-1 transcription factor subunit proto-oncogene JUND in human preimplantation embryos. Overall, we propose that MICA will be an informative method to make gene regulatory network predictions in other challenging-to-study biological contexts with limitations in the number of cells that can be analysed.

Results

Assessing the conditions for optimal GRN inference on synthetic data

We generated synthetic gene-expression data with known ground-truth GRN structure for a variety of sample sizes (see Methods) to determine the characteristics of the transcriptomic data on which GRN inference methods perform best and, importantly, to compare these conditions with our human blastocyst scRNA-seq datasets (see Fig. 1A). We then applied four different GRN prediction strategies to the simulated transcriptomes (see Methods for more details). 1) We applied GENIE3 (Aibar et al., 2017; Huynh-Thu et al., 2010), a random forests regression approach which takes into account expression levels of the regulated or target gene and is used for regulatory network inference in the SCENIC GRN prediction pipeline (Aibar et al., 2017; Kang et al., 2021; Marbach et al., 2012; Nguyen et al., 2021; Pratapa et al., 2020; Stone et al., 2021). 2) We compared this to the target gene approach using the L0L2 sparse penalised regression model (Hazimeh and Mazumder, 2018; Tibshirani, 1996) which minimizes the total size of the linear model coefficients so that a minimal set of regulatory TFs receive the largest linear model coefficients. 3) We also compared with the correlation coefficient as a reference: we used Spearman's rank correlation coefficient (Fieller et al., 1957) as we expect non-linear associations in the data. 4) Lastly, we applied a non-linear alternative measure of pairwise association based on mutual information (MI) that we speculated may be more appropriate for non-linear response functions in single-cell data (Faith et al., 2007; Krishnaswamy et al., 2014) (Fig. S1A). For the MI method, we used the empirical distribution of the MI values for each gene (Faith et al., 2007). We also varied the number of transcriptional regulators of each target gene in the synthetic data, to study the impact of this parameter on their performance. Further details of the analysis methods and step-by-step code are also available at: https://github.com/galanisl/early_hs_embryo_GRNs

Two main conclusions emerged from these simulations. First, using synthetic datasets, the performance of all methods increases from the sample size of $n = 10$ to $n = 1000$, as assessed statistically by the area under the receiver operating characteristic curve (AUROC) (Fig. 1B). However, we noted that the prediction accuracy of the GRNs only marginally improves as the number of cell samples surpasses $n = 100$ (Fig. 1B). Therefore, while sample size is important, increasing this beyond a threshold sample size does not further improve inference of the predicted transcriptional regulations. We further note that low sequencing depth (such as in 10x Genomics single-cell studies) may increase this optimal value of n. Second, limiting the number of potential transcriptional regulators of a target gene positively impacts the ability of a chosen inference method to recover the ground-truth GRN (Figs. 1B,C). From our simulations, 50 or fewer TFs yield the highest AUROC values for $n < 100$ (Fig. 1B). This would be a reasonable prediction for a given gene in a specific cell type based on our analysis of low input chromatin accessibility (CA) data from the human blastocyst (Liu et al., 2019), where the median number of TF motifs per gene is 35 for the inner cell mass (ICM) and 40 for the TE (Fig. S1B).

Based on these results and given the size of our human blastocyst datasets (Fig. 1C EPI: 26 cells, PE: 33 cells, TE: 45 cells with 1,366 TFs among 25,098 genes (Blakeley et al., 2015; Petropoulos et al., 2016; Yan et al., 2013)), we reasoned that TF-gene interactions predicted from experimentally collected gene expression data could be refined with complementary, context-specific epigenomic datasets. Specifically, we used low-input CA analysis of human blastocyst TE cells and the inner cell mass (ICM), comprised of EPI and PE cells, to refine the GRNs of the respective cell types with putative cis-regulatory interactions (Liu et al., 2019). Peak calling and annotation were performed with nf-core/atacseq to identify regions of open chromatin (Ewels et al., 2020). TF motif enrichment analysis in these open regions of open chromatin were identified using rgt-hint with TF binding models from HOCOMOCO and JASPAR (Li et al., 2019). Finally, the open chromatin regions enriched for TF motifs along with the predicted downstream target genes were determined based on the nearest transcriptional

start sites (most distances ranging from -5kbp to 10kbp). This narrowed down the number of genes (to 12,780 for EPI and PE, 12,981 for TE) and TFs (514) in the datasets, thus bringing our sample sizes and potential TFs per gene to the ranges suggested by our simulations.

Statistical evaluation of inferred human blastocyst GRNs

We next integrated the single-cell transcriptome data (Fig. S1C) from human blastocysts generated using the SMART-seq2 library preparation protocol (Blakeley et al., 2015; Petropoulos et al., 2016; Picelli et al., 2014; Yan et al., 2013) where fewer cells are sequenced but better transcript coverage and sequencing depth is obtained (~15,000 genes and ~7 million reads per cell) compared to more conventional scRNA-seq methods, such as 10x Genomics (~3,000 genes and ~50,000 reads per cell) (Wang et al., 2021). Due to the lack of genome-scale experimentally derived GRNs in the human embryo context, we evaluated the robustness of the predictions made by four inference approaches (L0L2 regression, GENIE3, Spearman correlation and MI) using three different strategies (see Methods). Since we did not find reports about the impact of gene expression normalisation choice on GRN predictions, we also assessed this parameter and considered the application of GRN predictors to log(TPM+1), log(FPKM+1), log-count and batch-corrected expression data.

We calculated a reproducibility score *R* for each putative regulatory interaction following the application of the network inference methods to human blastocyst data (see Methods) and investigated the distribution of the reproducibility values for the top-100,000 predicted edges (Figs. 2A and S2). The reproducibility estimator *R* estimates the posterior probability of seeing a network edge given the data; it quantifies the robustness or stability of the inference of this network edge. The accuracy quantified by the *R* reproducibility statistic relates to the stability of the model predictions to perturbation of the data. Fig. 2A reports the difference between the median of this distribution and the median of the distribution produced by a predictor that generates a random ranking of all possible TF-gene interactions (ΔR). We found that the most reproducible regulatory interactions were inferred by MI followed by a filtering process in which only TF-gene associations supported by CA data were considered in the final network (MICA) (Fig. 2A). As predicted by our simulations, the size of each cell type-specific dataset had a clear impact on GRN inference with methods such as GENIE3 producing more reproducible interactions in the TE. Interestingly, most inference methods produced better results with gene expression values following log(TPM+1) or log(FPKM+1) normalisation (Fig. 2A).

We also assessed robustness at the level of network structures, features, or subnetworks. To do so, we randomly split each dataset (EPI, PE and TE) into two groups with the same number of cells, then applied the inference methods to each one (with or without CA refinement), and finally benchmarked them either focussing on the top regulatory interactions (early recognition) or on all regulatory interactions (see Methods). We repeated this 10 times for 10 random splits of the data. For the first comparison, we identified the top 1% (by network score) of all possible regulatory interactions from each group, and then quantified the overlap of these top interactions between the groups using the area under the precision-recall curve (AUPRC) (Figs. 2B and S3). By comparing the differences between the median of ten resulting AUPRCs for each method to the random predictions described above, we found that MICA outperformed the other network prediction approaches and gave the highest difference in AUPRC when applied to log(TPM+1)- and log(FPKM+1)-normalised expression values (Fig. 2B). For the second comparison, we divided the data into two portions and then calculated a normalised L2 loss between the network scores over the whole network, rather than just the top 1% of interactions (Figs. 2C and S4). We found that the inverse value of this metric also confirms the robustness of MICA (Figs. 2C and S4).

Overall, our statistical evaluation strategies showed that the most robust GRN inference method to analyse the limited number of human blastocyst cells was MICA. Importantly, if

transcriptome-based predictions are not refined with CA data, most methods perform just slightly better than random (Figs. 2 and S2-S4), underscoring the importance of integrating multi-omics analysis in inference models. It was also important to assess the impact of gene expression normalisation on GRN prediction because we observed apparent effects in our benchmarks depending on the normalisation method used, with log(TPM+1) or log(FPKM+1) being the most suitable gene expression units in this context.

Association of inferred GRNs to human blastocyst cell lineages

We next evaluated the inferred GRNs to determine if they could recapitulate interactions of molecular markers of the three cell types that comprise the human blastocyst. First, we computed the overlap between the GRN edges predicted by each inference method for each blastocyst cell type to identify interactions associated with the EPI, PE and TE, as well as the interactions common to the three cell types (see Methods). We then used the out-degree of NANOG, GATA4 and CDX2, TFs which respectively mark the EPI, PE and TE (Figs. 3A,B), as a proxy for their activity in each one of the four networks. Our prediction is that these TFs should be actively regulating genes in the cell type-specific networks and participate in only a few interactions in the common GRN, based on their known expression pattern in the blastocyst and function in other mammalian contexts such as the mouse (Arceci et al., 1993; Chambers et al., 2003; Dietrich and Hiiragi, 2007; Mitsui et al., 2003; Niakan and Eggan, 2012; Roode et al., 2012; Strumpf et al., 2005). The common network did not show marker activity in the predicted GRNs (Figs. 3B and S5-S8), which is expected given that the expression of these markers is known to be mutually exclusive at this stage. The expected pattern for NANOG (active in the EPI and inactive in the PE and TE, Fig. 3A), was observed in the GRNs with TF-gene interactions supported by CA data and inferred with GENIE3, Spearman correlation and MI when applied to batch-corrected, FPKM and TPM data with some instances of the non-refined L0L2, GENIE3 and Spearman GRNs also matching the expected pattern (Fig. 3B). In the PE, the expected activity pattern for GATA4 (active in the PE and inactive in EPI and TE, Fig. 3A) and lack of detectable networks for NANOG and CDX2, were predicted by applying GENIE3+CA, Spearman correlation+CA and MICA to the FPKM and TPM datasets (Fig. 3B). Finally, the TE-expected pattern for CDX2 (active in the TE and inactive in the EPI and PE) and lack of detectable network for NANOG and GATA4, Fig. 3A) was only observed when using Spearman correlation or MICA on log-counts and batch-corrected data, MICA or MICA+CA on FPKM or TPM data (Fig. 3B). L0L2, with or without CA refinement, consistently performed poorly at predicting GRNs compared to the other methods used. Log-count normalisation failed to recover cell type specific GRNs for these TFs.

We next manually curated a list of gene sets representing the most relevant pathways and biological processes in the EPI (e.g., regulation of pluripotency) and the TE (e.g., embryonic placenta development) to perform a gene set enrichment analysis with the genes involved in the 500 regulatory interactions with the best prediction scores in the EPI and TE GRNs of the 25 most active TFs (Tables S1, S2, Methods). We restricted this analysis to the EPI and TE, because similar lists of gene-sets were not available for PE, where it is currently unclear which pathways are most relevant to this cell type. Next, we computed a validation score *V* as the number of relevant gene sets that were enriched at a significance level of 10% ($p<0.1$) in the EPI and TE GRNs (Fig. S9). We note that a low significance level was set because the resulting inferences are aggregated, mitigating the effect of false positive hits for individual gene groups. To facilitate the comparison between *V* scores across GRNs from different inference and normalisation methods, we normalised this score to the maximum score attained at the cell type level (Fig. 3C). We found that the CA-refined data agree better with the cell type-specific gene sets for both the top-predicted EPI and TE interactions, i.e. the interactions with the highest prediction scores (Fig. 3B). The GRNs inferred by Spearman+CA produced the highest *V* scores in the EPI and TE, and these were not impacted by the normalisation method employed. The second-best inference method was MICA, with

consistent *V* scores across normalisation methods. We note that both MICA and Spearman+CA are non-linear methods which do not involve regression, indicating that advanced regression methods may not be the most effective choice for biological discovery with these restricted sample-sizes. Taken together, both biological evaluation metrics that we considered confirmed the importance of refining single-cell transcriptome-based GRN inferences with CA data and underscored the robustness of MICA in predicting GRNs from the analysed human blastocyst datasets. Based on these results, we decided to focus on the GRNs predicted by this method for the analyses presented in the following sections.

Predicted TF networks for NANOG, GATA4 and CDX2

Using MICA, we constructed GRNs for TFs expressed in the EPI, PE and TE. All MICA GRN predictions can be found on FigShare: doi.org/10.6084/m9.figshare.21968813. For visualization, the predicted GRN for each of the TFs is separated into target and regulator TF networks. Target networks contain a maximum of 25 top potential target TFs of the hub (or central) TF, whereas regulator networks include a maximum of 25 top TFs that potentially regulate the hub. The average expression of the network members across samples of the cell type of interest is represented by the size of the node. MI scores are represented by the thickness of the edges in the network and edge colour highlights. To further refine the MICA-predictions we used the Spearman's rank correlation coefficient between the expression levels of the source and target nodes across samples of the cell type of interest to define correlated or anti-correlated expression. Correlated or anti-correlated node pairs correspond to positive or negative Spearman's rank coefficient with p-value smaller than 0.1, whereas node pairs having p-value equals or larger than 0.1 were defined as uncorrelated.

Among the top NANOG targets, TFs RREB1, NCAO3, ZNF343, ZFP42, and NME2 are predicted to be positively regulated by NANOG (Fig. 4A). ZFP42 is a pluripotency marker encoding the REX1 protein and has been shown to be a direct target of NANOG in mouse pluripotent stem cells (Shi et al., 2006). ZNF343 is a less well-characterized TF, but multiple NANOG ChIP-seq datasets in both naïve and primed human embryonic stem cells (ESCs) showed high binding score (MACS2 score > 1000) in the proximal region of the transcription start site (TSS) of ZNF343 (Fig. S10A; (Barakat et al., 2018; Chovanec et al., 2021; Lyu et al., 2018)), which suggests direct regulation of ZNF343 by NANOG. Interestingly, NME2 was previously predicted to be a regulator instead of a target of NANOG in mouse pluripotent stem cells using the TENET GRN inference method (Kim et al., 2021). This inconsistency may be due to the lack of chromatin accessibility data for robust directionality inference in the TENET method, or a species difference. Indeed, some mouse naïve pluripotency regulators, such as ESRRB, which is also a direct target of NANOG in mouse pluripotent stem cells (Festuccia et al., 2012), were not expressed in the human EPI (Blakeley et al., 2013). Putative regulators of NANOG predicted from our MICA network analysis contain multiple KLF factors, including KLF3, KLF5, KLF9 and KLF16 (Fig. 4B). Spearman correlation analysis suggest that KLF9 and KLF16 potentially down-regulate NANOG expression, based on their anti-correlated expression, whereas KLF3 and KLF5 are identified as potential regulators of NANOG by MICA, but not significantly correlated by Spearman correlation.

In the PE, GATA4 was predicted to positively regulate the expression of SP8, TET1, and SKIL while repressing the expression of ELF3, TFDP2 POGK, ZNF770, and NR2F2 (Fig. 4C). It is also predicted to be a target of HNF1B and SALL4 and repressed by ETV4 and E2F6 (Fig. 4D). These interactions have not been experimentally validated or inferred. However, NR2F2 was previously identified as a maturation marker of polar TE (Meistermann et al., 2021). The repression of NR2F2 by GATA4 predicted in the PE suggests a role for GATA4 in maintaining the PE cell identity by inhibiting the polar TE program. Furthermore, it has been shown that SALL4 is required for mouse PE-derived extra-embryonic endoderm cell derivation and knockout of SALL4 in these cells cause down-regulation of GATA4 (Lim et al., 2008). In

addition, multiple endoderm genes such as GATA4, GATA6, and SOX17 were shown to be SALL4-bound genes by ChIP-seq (Lim et al., 2008). These findings are consistent with the inferred GATA4 regulatory network.

Interestingly, TBX3 is a target of CDX2 (Fig. 4E), and the role of TBX3 has been implicated in trophoblast cell differentiation (Lv et al., 2019). CDX2 is predicted to be regulated by both KLF5 and KLF6, which are also molecular markers of the trophectoderm lineage (Fig. 4F). KLF5 is necessary for trophectoderm formation in the mouse pre-implantation embryo and is required for CDX2 expression in mouse ESCs (Ema et al., 2008; Lin et al., 2010). Interestingly, further analysis of the CDX2 interactions showed that TBX3 and FOXH1 are also potential positive regulators of KLF5 and KLF6. Positive feedback loops are predicted between CDX2, TBX3 and KLF5, as well as CDX2, FOXH1 and KLF6 (Fig. S10B). Other key developmental regulators including HAND1, GATA3 and GATA6, are also predicted to regulate CDX2 expression (Fig. 4F). This is consistent with the timing of GATA3 protein expression preceding that of CDX2 (Gerri et al., 2020). Further investigation will be needed to understand the differences between the CDX2-high and CDX2-low TE cells and how the positive feedback loops formed within the CDX2 network enhance and stabilize CDX2 expression in the CDX2-high population.

Maintenance of TFAP2C expression by JUND in all lineages of human blastocyst

We next sought to determine if the MICA network modelling predicts novel interactions or associations between TFs in early human embryo development. We focused on TFAP2C as an example for the network comparison. TFAP2C is a molecular marker that is initially expressed in all the cells at the morula stage in mouse embryos and later specifically restricted to the TE at the blastocyst stage and it is not expressed in other lineages (Cao et al., 2015; Gerri et al., 2020). However, in human embryos, TFAP2C is expressed in the TE, EPI and PE at the blastocyst stage (Blakeley et al., 2015) and has been shown to maintain pluripotency in naïve human embryonic stem cells by regulating OCT4 expression (Chen et al., 2018; Pastor et al., 2018). By performing comparisons of TFAP2C networks in human EPI, TE, and PE cells, we found a conserved putative interaction consisting of TFAP2C, JUND, SOX4, and GCM1 (Fig. 5A). In addition, all four factors showed significant positive correlations in their expression (Figs. 5B, S11). MICA predicts that JUND and SOX4 regulate TFAP2C, while TFAP2C targets GCM1 in all three lineages. In the EPI and PE, SOX4 and GCM1 formed a feedback loop. Interestingly, in the TE, the correlation between GCM1 and SOX4 is absent, and SOX4 is predicted to target JUND, which in turn may regulate TFAP2C. Our network predicts that interactions between these four TFs maintains TFAP2C expression in all three lineages.

To determine if TFAP2C and JUND protein expression is positively correlated in embryos, as predicted by MICA, we performed immunofluorescence analysis of human preimplantation blastocysts approximately 6.5 days after fertilisation. We observed that TFAP2C and JUND were co-expressed in cells of the human blastocysts (Fig. 5C, S13A; n=4). We next performed 3D nuclear segmentation and calculated the Pearson correlation coefficient between TFAP2C and JUND based on the DAPI-normalized protein intensity (Fig. 5D). TFAP2C intensity showed a linear increase with the increase of JUND intensity in all analysed human embryos, and their intensities are highly correlated (0.68-0.85 Pearson correlation; $p < 0.001$; Fig. 5D). Overall, this demonstrates the informativeness of the MICA network analysis to predict correlations and possible regulatory relationships between transcription factors that can be experimentally tested.

In addition to the MICA predictions, we also performed Spearman correlation analysis of the significant edges identified by the MICA analysis. Surprisingly, around half of the interactions are in non-linear fashion, highlighting the informativeness of MICA to capture complex non-

monotonic dependencies. From the TFAP2C network predicted in the EPI lineage, we found that TFAP2C potentially regulates FOXO3 and ZFP42 in a non-linear manner (Fig. S12). The expression of FOXO3 and ZFP42 seems to fit better with the expression of TFAP2C on an exponential curve rather than a linear line between TFAP2C and JUND (Fig. S13B). This suggests that when analysing scRNAseq or low input multi-omics analyses similar non-linear correlations may exist and this may have biological significance. It would be interesting to know whether and which types of non-linear interaction predominate and the biological significance of these non-linear regulations.

Discussion

The relationship between genome-wide transcriptomic and epigenomic changes and cell fate specification in human embryogenesis is unclear. Studies of human pre-implantation development rely on the donation of surplus embryos derived from assisted reproduction technologies, and the use of such embryos for research is tightly regulated and subject to significant limitations, such as a lack of ability to conduct such research in some jurisdictions (Niakan et al., 2012). In addition, the collection of single cells from such precious embryos is technically challenging and requires specialist expertise and micropipettes to disaggregate microscopic embryos. Therefore, currently available -omics datasets from human blastocysts comprise only a few tens of samples per cell type and are therefore very limited. This contrasts with single-cell analyses in other cellular and developmental contexts that are based on tens of thousands of samples (or more) per cell type (Zheng et al., 2017).

Sample size is one of the most important considerations when selecting or designing statistical methodology, for example to infer networks of regulations of TFs and their target genes. Hence, GRN inference in -omics data from human pre-implantation embryos presents unique statistical challenges. In particular, methodology that can leverage information about gene regulations from small sample-sizes is required for this context. On the other hand, the lack of heterogeneity in early human embryos compared to adult tissue makes this a good context in which to assess GRN inference methodologies, because there is less unmeasured variability arising from environmental factors. To assess whether GRN inference method can be informative in this challenging-to-study context, we have systematically compared several popular methodologies. Furthermore, we have tested how incorporation of complementary cis-regulatory epigenomic data from ATAC-seq improves GRN inferences. Consistent with other contexts (Argelaguet et al., 2022; Kamimoto et al., 2020), we found that incorporating chromatin accessibility/TF motif analysis together with transcriptional inferences improves the accuracy of GRN inference, by first narrowing down the choice of TF targets from which to infer the mRNA transcript co-expression network, a principle that is likely to be especially important with small sample sizes. Notably, we analyse RNA-seq data generated using SMART-seq2 and the sequencing method and depth of sequencing will likely impact on the choice of GRN inference method.

Here we showed that incorporating complementary epigenomic data with transcriptomic data improves the reproducibility of inferred GRNs. Furthermore, it has enabled us to make predictions about GRNs operational in early human embryos that are consistent with an understanding of the function and association of the regulators in other developmental and stem cell contexts. We suggest that for network inference using advanced regression methods, it may be preferable to pre-filter using epigenomic data to first narrow down the TF targets in scRNA-seq datasets, because this gives the network inference algorithm an easier time of selecting the regulators from transcriptome data, which is consistent with the experience of others using alternative GRN prediction methods (Fleck et al., 2022; Kamimoto et al., 2020; Kartha et al., 2022) . Alternative methods incorporate epigenomic data after inference of the mRNA transcript co-expression network (González-Blas et al., 2022) and this has been applied successfully to infer GRNs in the fly brain (Janssens et al., 2022). It will be

interesting to determine how the type and sequential order of incorporating multi-omics datasets impacts on GRN predictions.

We also note some limitations on the interpretation of the GRNs predicted. For example, one ATAC-seq peak could cover multiple transcription factor binding sites in a region. In such cases, we include all TFs with motifs mapping to this region as potential regulators of the gene with the closest TSS (transcriptional start site) to the region, for subsequent transcript co-expression network modelling. However, it will be interesting to determine if this can be refined, by applying the recently developed chromVAR-Multiome method to human blastocysts to generate an *in silico* ChIP-seq library for this context (Argelaguet et al., 2022). Moreover, the ATAC-seq data applied in this study analysed the ICM data in bulk, without distinguishing between EPI and PE cells. Therefore, cell-type specific chromatin accessibility could not be considered, and specific interactions may have been missed due to the heterogeneity of the data or if the ICM CA data failed to reflect developmentally cis-regulations of more developmentally progressed EPI and PE cells. In addition, predictions based on the nearest TSS will miss long-range enhancers that are known to be important for gene regulation (Schoenfelder and Fraser, 2019). In the future, integration of single-cell or nuclei matched transcriptome and ATAC-seq chromatin accessibility data, like recent studies in the mouse (Argelaguet et al., 2022), would be preferable to apply in the human blastocyst context. We note that the GRN interference methods predicted edges that overlap between the four inference methods. Identifying overlapping inferences by comparing more than one GRN inference method may be a strategy to identify network edges with more confidence due to the agreement between several inference methodologies. However, this strategy may also miss some edges which can only be detected by one method and not another.

We also note that so far, we have separately modelled GRN structure to specific pre-implantation embryonic cell types constrained to a single developmental time-point. In the future, we seek to model dynamic GRN structure in transcriptionally distinct human blastocyst lineages. Moreover, we seek to integrate CUT&RUN or CUT&Tag TF-DNA binding analysis (Kaya-Okur et al., 2019; Meers et al., 2019; Skene and Henikoff, 2017) for key putative developmental regulators, such as GATA3, to further narrow down experimentally validated occupancy from the ATAC-seq predictions we used in this study, similarly to a recent application in mouse blastocysts (Hainer et al., 2019; Hayashi and Inoue, 2023), though we note that in this context TF occupancy studies will be restricted to a few TFs with good quality antibodies. It will also be important to determine which cis regulatory regions are required for target gene regulation through systematic perturbation studies.

In summary, the MICA network analysis pipeline we developed is a tool that can be applied to challenging-to-study developmental contexts with limited sample size, such as the human blastocyst, to make predictions about TF interactions that can be experimentally tested in the future. As more datasets become available, we anticipate that the networks predicted will be further refined.

Methods

Ethics statement

All human embryo experiments followed all relevant institutional and national guidelines and regulations.

This study was approved by the UK Human Fertilisation and Embryology Authority (HFEA): research licence number R0162, and the Health Research Authority's Research Ethics Committee (Cambridge Central reference number 19/EE/0297).

The process of licence approval entailed independent peer review along with consideration by the HFEA Licence and Executive Committees. Our research is compliant with the HFEA code of practice and has undergone inspections by the HFEA since the licence was granted. Research donors were recruited from patients at Bourn Hall Clinic, Homerton University Hospital, The Bridge Centre and IVF Hammersmith.

Informed consent was obtained from all couples that donated surplus embryos following IVF treatment. Before giving consent, people donating embryos were provided with all of the necessary information about the research project, an opportunity to receive counselling and the conditions that apply within the licence and the HFEA code of practice. Donors were informed that, in the experiments, embryo development would be stopped before 14 days post-fertilization, and that subsequent biochemical and genetic studies would be performed. Informed consent was also obtained from donors for all the results of these studies to be published in scientific journals. No financial inducements were offered for donation. Consent was not obtained to perform genetic tests on patients and no such tests were performed. The patient information sheets and consent document provided to patients are publicly available (https://www.crick.ac.uk/research/a-z-researchers/researchers-k-o/kathy-niakan/hfea-licence/). Donated embryos surplus to the IVF treatment of the patient were cryopreserved and were transferred to the Francis Crick Institute where they were thawed and used in the research project.

ATAC-seq data processing and analysis

Chromatin accessibility profiles from the inner cell mass (ICM) and TE were obtained from the data produced by Liu *et al.* with the LiCAT-seq protocol (Liu et al., 2019). Alignment to the reference genome (GRCh38), peak calling and annotation were performed with nf-core/atacseq v1.1.0 (Ewels et al., 2020). Then, we carried out footprinting followed by TF motif enrichment analysis in the regions of open chromatin using rgt-hint v0.13.0 with TF binding models from HOCOMOCO and JASPAR (Li et al., 2019). Finally, we associated the TFs that exhibited over-represented motifs in these regions with their closest transcription starting sites (most distances ranging from -5kbp to 10kbp).

scRNA-seq data processing and analysis

We integrated scRNA-seq data from three different studies (Blakeley et al., 2015; Petropoulos et al., 2016; Yan et al., 2013) focusing on the three cell types present at the late blastocyst stage (Fig. 1, Fig. S3A). Cell type annotations were taken from the work by Stirparo *et al*. Alignment to the reference genome (GRCh38) and calculation of gene counts and TPM-normalised counts were performed on each dataset separately with nf-core/rnaseq v1.4.2 (Ewels et al., 2020). The resulting gene expression matrices were integrated and normalised (log-counts and batch-corrected counts) using Bioconductor tools (Amezquita et al., 2019). The final set of cells was manually curated based on the UMAP representation of the batch-corrected data (see Fig. S3 and Table S1). The list of 25,098 genes in the expression matrices was reduced to the unique set of TFs and transcription starting sites (TSS) derived from the motif enrichment analysis applied to the ATAC-seq data. We used the ICM TFs and TSS for the EPI and PE matrices (12,780 genes) and the TE TFs and TSS for the TE matrices (12,981 genes).

Network inference methods

For network inference, we compared the best performing strategy in the DREAM5 challenge, GENIE3 (Huynh-Thu et al., 2010), with a non-linear alternative based on MI (Faith et al., 2007), the Spearman's rank correlation coefficient, and the L0L2 sparse regression method that we applied using recent advances in sparse multivariate statistical modelling (Bartlett et al., 2019; Hazimeh and Mazumder, 2018), as follows.

For GENIE3, transcription factors are ranked according to the degree of variability in their expression level and how the expression of the putative regulator correlates with a target gene. This ranking is then used to construct the co-expression network for all genes and transcription factors, by thresholding the algorithm's variance reduction score at the tenth percentile of its empirical distribution. The GRN is then inferred as the intersection of the edges in this co-expression network with the edges in the network of all possible gene regulations derived from the chromatin accessibility / DNA binding motif data. This network of all possible gene regulations is defined as all network edges from regulating TF to regulated gene, where an edge represents a DNA binding motif for the TF in regulatory DNA within open chromatin in the regulated gene. For GENIE3, all default settings were used.

With the Spearman correlation coefficient, a weighted co-expression network is inferred as the absolute value of the correlation coefficient. The gene regulatory network is then inferred as the intersection of the edges in this co-expression network with the edges in the network of all potential gene regulations derived from the chromatin accessibility / DNA binding motif data.

For L0L2 regression (described in more detail below), the model automatically chooses a ranked subset of TFs from those predicted as regulators of the target gene in the chromatin accessibility / DNA binding motif data inferences. In this way, each target gene takes its turn for a model to be fitted around that target gene. After the model has been fitted to every target gene, the global gene regulatory network can be constructed by combining the local networks fitted around each target gene. For L0L2 regression, sparsity hyperparameters were chosen using the L0Learn package's internal cross-validation.

In more detail, for L0L2 regression we start with a linear model of the expression level y of the regulated target gene (Dobra et al., 2004), in terms of the expression levels $x_1, x_2, \ldots, x_p$, of p transcription factors. We want to use the size of the fitted model coefficients b_1, b_2, etc. to measure the strength of regulation of the target gene by transcription factors (TFs) 1, 2, etc. We use sparse regression to find b_1, b_2, etc., as this specifically minimises the number of non-zero model coefficients, by requiring that the coefficients b_q are set to zero as much as possible. This leads to a more parsimonious model, in which a relatively small number $p' \ll p$ of transcription factors is inferred to be regulating the target gene, as a result of non-zero b_q. Sparse regression minimizes:

$$[\, y - (a + b_1x_1 + b_2x_2 + \ldots + b_px_p)\,]^2 + \psi, \qquad (1)$$

where ψ 'penalises' models with values of b_q (q=1,…,p) further from zero. The most popular choices for ψ include $\psi = \lambda \Sigma b_j^2$, which is called 'ridge regression' (L2 regression), and $\psi = \lambda \Sigma |b_j|$, which is called 'the lasso' (L1 regression). It can be shown that Eq.1 is equivalent to applying the constraint $\Sigma b_j^2 < t^2$ for $\psi = \lambda \Sigma b_j^2$ (L1 regression) or $\Sigma |b_j| < t$ for $\psi = \lambda \Sigma |b_j|$ (L0 regression). Then, 'best-subset regression' (L0 regression) specifies the number of transcription factors that can have non-zero b_j. It does this by using the constraint $\Sigma b_j^{\,0} \leq k$, which is equivalent to $\psi = \lambda \Sigma b_j^0$ in Eq.1. Combinations of these constraints are also often more effective, such as L1L2 regression (also called 'the elastic net' (Zou and Hastie, 2005), which was very successful in genomics), with penalty term $\psi = \gamma \Sigma |b_j| + \lambda \Sigma b_j^2$. Recently, L0L2 regression has been proposed as an improvement (Hazimeh and Mazumer, 2018), with penalty term $\psi = \gamma \Sigma b_j^0 + \lambda \Sigma b_j^2$. We use L0L2 regression in this study, for reasons as follows. Sparse regression using the L0 penalty is an ideal model for inferring a minimal set of regulating transcription factors, because it specifically selects the best set of k transcription factors for the model (i.e., the 'best subset', of the available transcription factors). Combining with the L2 penalty in L0L2 makes the model better specified for the data, by minimizing the total size of the linear model coefficients so that the most important TFs receive the largest linear model coefficients. We use sparse L0L2 regression to infer the best subset of regulators

of each target gene, from the full list of TF-gene associations supported by the chromatin accessibility data.

For MI-based inference, the co-expression network is estimated first, as follows. We use an empirical estimate of the distribution of the MI values for each gene (Daub et al., 2004; Faith et al., 2007). Writing the estimated MI between the expression levels of genes x and y as M_{xy}, we calculate the approximately $N(0,1)$ distributed variable z_{xy} according to the equation:

$$Z_{xy}^2 = F^{-1}\,[\Phi_{y|x}\,(M_{xy})\,]^2 + F^{-1}\,[\Phi_{x|y}\,(M_{xy})\,]^2\ ,$$

where F is the $N(0,1)$ cumulative distribution function (c.d.f.), and $\Phi_{x|y}$ and $\Phi_{y|x}$ are the empirical c.d.f.s of M_{xy} conditioned on x and y, respectively. From these $N(0,1)$ distributed variables z_{xy}, we calculate p-values, and then threshold at a false discovery rate of 5%. Again, the gene regulatory network is inferred as the intersection of the edges in this co-expression network with the edges in the network of all possible gene regulations derived from the chromatin accessibility / DNA binding motif data.

We also considered a "random predictor" that outputs a random ordering of all the possible TF-gene interactions.

The putative regulatory links predicted by each of these methods using the scRNA-seq data were evaluated *as is* but also subjected to a filtering process in which only TF-gene associations supported by the chromatin accessibility data were considered in the final network (for GENIE3, MI and Spearman correlation methods). In the case of L0L2 sparse regression, only TF-gene associations supported by the chromatin accessibility data were considered as potential regulators of the target gene in the regression model. To identify these refined predictions, we added the *+CA* suffix to the name of the GRN inference methods. In both cases, to generate the final network, we selected the top 100,000 edges by ranking edges according to their network score. We define network score as the absolute correlation coefficient or linear regression coefficient (in the case of Spearman's correlation and sparse regression respectively), or as -log10p for mutual information, or the GENIE3 score.

Simulation study

For our simulation study, we used the `daggitty` package in `R` to generate synthetic gene expression data based on pre-defined GRNs with pre-determined network structure. These GRNs were generated with network edge density of ρ=0.07, i.e., 7% of all possible edges (or gene regulations), are present in the network (this value was estimated from the available ATAC-seq+TF motif data). The synthetic datasets were generated with a range of sample size n and number of potential regulators of each node (gene) p, using linear models, as follows. For each combination of n and p, we generated 100 GRNs; then corresponding observed gene-expression data-sets were generated for each of the GRNs by specifying that the expression level of a downstream gene should depend on a linear combination of the expression levels of its upstream regulators:

$$x_d = b_1{*}x_{u1} + b_2{*}x_{u2} + b_3{*}x_{u3} + \ldots\ b_g{*}x_{ug} + e,$$

where x_d is the expression level of the regulated (downstream) gene, and $x_{u1\ \ldots}\ x_{up}$ are the expression levels of the g regulating (upstream) TFs, b_1, b_2 … b_g are linear model coefficients, and e is random noise. The different network inference methods (GENIE3, L0L2 sparse regression, MI, Spearman correlation) were then applied to these generated data, and the results were compared with the known pre-determined network structure. This comparison was assessed by the AUC statistic, the 'area under the ROC (receiver-operator characteristic) curve'.

699 **Statistical evaluation metrics**
700
701 We calculated a reproducibility score *R* as a bootstrap estimate of the posterior probability of
702 observing an edge *E* given the dataset *D*, $R=P(E|D)$ (Pe'er, 2005), for the top 100,000
703 predicted edges. We also carried out 2-fold cross-validation in two ways as follows. We
704 randomly split each dataset (EPI, PE and TE) in two groups with the same number of cells ten
705 times (repeated 2-fold cross-validation), applied the inference methods (with or without
706 chromatin accessibility refinement), took the top-1% of all possible regulatory interactions from
707 one group and quantified the extent to which the top interactions inferred from the other group
708 coincide with that reference using the area under the precision-recall curve (AUPRC). In
709 addition, we calculated a normalised L2 loss comparing all the network inferences from the
710 two network fits on the 2 folds of the data (at the level of the network scores). The normalised
711 L2 loss is then defined as the L2 loss comparing the network scores from each of the 2 data
712 folds, divided by the product of the square roots of the L2 norms of the network scores of each
713 of the 2 data folds.
714
715 **Biological evaluation metrics**
716
717 For each combination of inference method and normalisation approach, we computed the
718 intersection between the GRN edges predicted to identify interactions that are specific to the
719 EPI, PE and TE, as well as the interactions common to the three cell types. In set notation this
720 corresponds to EPI-specific = (EPI \ PE) \ TE, PE-specific = (PE \ EPI) \ TE, TE-specific = (TE
721 \ EPI) \ PE and Common = EPI $\cap$ PE $\cap$ TE. Then, we used the out-degree of NANOG, GATA4
722 and CDX2 (marker TFs of the EPI, PE and TE, respectively) as a proxy for their activity in
723 each one of the four networks. We considered that a marker was active if its normalised out-
724 degree (i.e., the proportion of all genes it regulates in that GRN) was at least the median
725 normalised out-degree across all networks.
726
727 We calculated a validation score *V* as the number of relevant gene sets that were enriched at
728 a significance level of 10% ($p<0.1$) in a gene-set enrichment analysis performed with the genes
729 regulated by the 25 most connected TFs and that were part of the 500 interactions with the
730 highest prediction scores produced by the GRN inference methods for the EPI and TE. The
731 list of gene sets for the EPI and TE were manually curated and represent the most relevant
732 pathways and biological processes in each one of these cell types (see Tables S1 and S2).
733 The starting list of gene sets comprised all the pathways and Gene Ontology Biological
734 Process (GO BP) terms collated by the Bader Lab at the University of Toronto on 01 October
735 2020
736 (http://download.baderlab.org/EM_Genesets/October_01_2020/Human/symbol/Human_GO
737 BP_AllPathways_no_GO_iea_October_01_2020_symbol.gmt). To facilitate the comparison
738 between *V* scores from different GRN inference methods within a cell type, we normalised *V*
739 to the maximum score attained by a network predictor for that cell type (i.e., EPI or TE).
740
741 **Human Embryo Culture**
742
743 Human embryos were cultured as previously described (Gerri et al., 2020). Vitrified human
744 blastocyst stage embryos were thawed using Kitazato Thawing Media (VT602, order number
745 91121) following the manufacturer's instructions.
746
747 Human embryos were cultured in drops of pre-equilibrated Global medium (LifeGlobal; LGGG-
748 20) supplemented with 10% human serum albumin (LifeGlobal; GHSA-125) and overlaid with
749 mineral oil (Origio; ART-4008-5P). Preimplantation embryos were incubated at 37 °C and 5%
750 CO_2 in an EmbryoScope+ time-lapse incubator (Vitrolife) and cultured for up to 24hrs for
751 human blastocyst.
752
753 **Immunofluorescence staining**

Embryos were fixed with freshly prepared 4% paraformaldehyde in PBS. Fixation was performed for 20 min at room temperature for embryos. Embryos were then washed 3 times in 1× PBS with 0.1% Tween-20 to remove residual paraformaldehyde. Permeabilization was performed with 1× PBS with 0.5% Tween-20 and followed by blocking in blocking solution (10% donkey serum in 1× PBS with 0.1% Tween-20) for 1 h at room temperature on a rotating shaker. Then, antibody incubation was performed with primary antibodies diluted in blocking solution overnight at 4 °C on rotating shaker. The following day, embryos and cell cultures were washed in 1× PBS with 0.1% Tween-20 for 3 times, and then incubated with secondary antibodies diluted in blocking solution for 1 h at room temperature on a rotating shaker in the dark. Next, embryos and cell cultures were washed in 1× PBS with 0.1% Tween-20 for 3 times. Finally, embryos were placed in 1× PBS with 0.1% Tween-20 with Vectashield and DAPI mounting medium (Vector Lab; H-1200) (1:30 dilution). Embryos were placed on μ-Slide 8-well dishes (Ibidi; 80826) for confocal imaging. The antibodies and concentrations used are reported in Table S3.

Confocal imaging

Confocal immunofluorescence images were taken with Leica SP8 confocal microscope. 2-μm-thick optical sections were collected for embryo Z-stack imaging.

Nuclei segmentation and quantification

Nuclei segmentation and quantification were performed on Z-stack confocal images taken at 2-μm-thick optical sections. Stardist (Weigert et al., 2020) was used for nuclei segmentation followed by CellProfiler (Stirling et al., 2021) for nuclei tracking and fluorescence intensity quantification based on a customized pipeline modified from Lea et al., 2021. First, LIF format confocal images were exported into multi-channel Z-stack TIF format for each Z-stack image using ImageJ (Schneider et al., 2012). Then, Stardist was used to identify the nuclei based on the DAPI channel (358 nm). Finally, Stardist outputs were split into single-channel single-stack images and loaded into the CellProfiler v4.2.5 to track nuclei across image slices and quantify the fluorescence intensity. Customized pipeline and scripts can be found here: https://github.com/galanisl/early_hs_embryo_GRNs

Data and code availability

scRNA-seq and ATAC-seq data were obtained from the European Nucleotide Archive [accession numbers: PRJNA153427, PRJNA277181, PRJEB11202 and PRJNA494280]. Data pre-processing and analysis scripts are available at https://github.com/galanisl/early_hs_embryo_GRNs.

Acknowledgements

We thank Zimeng Chen for contributing to the initial analysis of the synthetic datasets. We thank members of the Niakan lab for helpful discussions and feedback on the manuscript. Work in the laboratory of KKN was supported by the Wellcome (221856/Z/20/Z) and the Wellcome Human Developmental Biology Initiative (215116/Z/18/Z). Work in the laboratory of KKN was also supported by the Francis Crick Institute, which receives its core funding from Cancer Research UK (CC2074), the UK Medical Research Council (CC2074) and the Wellcome Trust (CC2074). The work carried out by TEB was partly supported by MRC grant (MR/P014070/1). For the purpose of Open Access, the authors have applied a CC BY public copyright licence to any Author Accepted Manuscript version arising from this submission.

Competing Interests

No competing interests declared.

Author contributions

GAL, TEB and KKN conceived the project. GAL and TEB developed the analytical network interference and statistical methods and analysed data. QH developed the network model representation pipeline, analysed data and performed immunostaining analysis and quantification. AM performed human embryo thaw and culture. CS provided advice on image quantification and analysed data. KKN analysed data and funded the project. KE, PS and LC coordinate the donation of embryos to the research project. GAL, TEB, QH, CS and KKN wrote the manuscript.

References

Aibar, S., González-Blas, C. B., Moerman, T., Huynh-Thu, V. A., Imrichova, H., Hulselmans, G., Rambow, F., Marine, J.-C., Geurts, P., Aerts, J., et al. (2017). SCENIC: single-cell regulatory network inference and clustering. *Nature Methods* 14, 1083–1086.

Amezquita, R. A., Lun, A. T. L., Becht, E., Carey, V. J., Carpp, L. N., Geistlinger, L., Marini, F., Rue-Albrecht, K., Risso, D., Soneson, C., et al. (2019). Orchestrating single-cell analysis with Bioconductor. *Nature Methods* 17, 137–145.

Arceci, R. J., King, A. A., Simon, M. C., Orkin, S. H. and Wilson, D. B. (1993). Mouse GATA-4: a retinoic acid-inducible GATA-binding transcription factor expressed in endodermally derived tissues and heart. *Mol Cell Biol* 13, 2235–2246.

Argelaguet, R., Lohoff, T., Li, J. G., Nakhuda, A., Drage, D., Krueger, F., Velten, L., Clark, S. J. and Reik, W. (2022). Decoding gene regulation in the mouse embryo using single-cell multi-omics. *bioRxiv* 2022.06.15.496239.

Barakat, T. S., Halbritter, F., Zhang, M., Rendeiro, A. F., Perenthaler, E., Bock, C. and Chambers, I. (2018). Functional Dissection of the Enhancer Repertoire in Human Embryonic Stem Cells. *Cell Stem Cell* 23, 276-288.e8.

Bartlett, T. E., Kosmidis, I. and Silva, R. (2019). Two-way sparsity for time-varying networks, with applications in genomics. *arXiv* arXiv:1802.08114.

Barzel, B. and Barabási, A.-L. (2013). Network link prediction by global silencing of indirect correlations. *Nature Biotechnology* 31, 720–725.

Blakeley, P., Fogarty, N. M. E., del Valle, I., Wamaitha, S. E., Hu, T. X., Elder, K., Snell, P., Christie, L., Robson, P. and Niakan, K. K. (2015). Defining the three cell lineages of the human blastocyst by single-cell RNA-seq. *Development* 142, 3151–3164.

Brandman, O. and Meyer, T. (2008). Feedback Loops Shape Cellular Signals in Space and Time. *Science* 322, 390–395.

Boroviak, T., Loos, R., Lombard, P., Okahara, J., Behr, R., Sasaki, E., Nichols, J., Smith, A., Bertone, P. (2015). Lineage-specific profiling delineates the emergence and progression of naïve pluripotency in mammalian embryogenesis. *Developmental Cell* 35, 366–82.

Butte, A. J. and Kohane, I. S. (1999). Mutual information relevance networks: functional genomic clustering using pairwise entropy measurements. In *Biocomputing 2000*, pp. 418–429. Honolulu, Hawaii, USA: WORLD SCIENTIFIC.

Cahan, P., Li, H., Morris, S. A., Lummertz da Rocha, E., Daley, G. Q. and Collins, J. J. (2014). CellNet: Network biology applied to stem cell engineering. *Cell* 158, 903–915.

Cao, Z., Carey, T. S., Ganguly, A., Wilson, C. A., Paul, S. and Knott, J. G. (2015). Transcription factor AP-2γ induces early Cdx2 expression and represses HIPPO signaling to specify the trophectoderm lineage. *Development* 142, 1606–1615.

Chai, L. E., Loh, S. K., Low, S. T., Mohamad, M. S., Deris, S. and Zakaria, Z. (2014). A review on the computational approaches for gene regulatory network construction. *Comput Biol Med* 48, 55–65.

Chambers, I., Colby, D., Robertson, M., Nichols, J., Lee, S., Tweedie, S. and Smith, A. (2003). Functional expression cloning of Nanog, a pluripotency sustaining factor in embryonic stem cells. *Cell* 113, 643–655.

Chan, T. E., Stumpf, M. P. H. and Babtie, A. C. (2017). Gene Regulatory Network Inference from Single-Cell Data Using Multivariate Information Measures. *Cell Systems* 5, 251-267.e3.

Chen, S. and Mar, J. C. (2018). Evaluating methods of inferring gene regulatory networks highlights their lack of performance for single cell gene expression data. *BMC Bioinformatics* 19, 232.

Chen, D., Liu, W., Zimmerman, J., Pastor, W. A., Kim, R., Hosohama, L., Ho, J., Aslanyan, M., Gell, J. J., Jacobsen, S. E., et al. (2018). The TFAP2C-Regulated OCT4 Naive Enhancer Is Involved in Human Germline Formation. *Cell Rep* 25, 3591-3602.e5.

Chovanec, P., Collier, A. J., Krueger, C., Várnai, C., Semprich, C. I., Schoenfelder, S., Corcoran, A. E. and Rugg-Gunn, P. J. (2021). Widespread reorganisation of pluripotent factor binding and gene regulatory interactions between human pluripotent states. *Nat Commun* 12, 2098.

Daub, C. O., Steuer, R., Selbig, J. and Kloska, S. (2004). Estimating mutual information using B-spline functions - an improved similarity measure for analysing gene expression data. *BMC Bioinformatics* 5, 118.

Davidson, E. H. and Erwin, D. H. (2006). Gene regulatory networks and the evolution of animal body plans. *Science* 311, 796–800.

Dietrich, J.-E. and Hiiragi, T. (2007). Stochastic patterning in the mouse pre-implantation embryo. *Development* 134, 4219–4231.

Dobra, A., Hans, C., Jones, B., Nevins, J. R., Yao, G. and West, M. (2004). Sparse graphical models for exploring gene expression data. *Journal of Multivariate Analysis* 90, 196–212.

Ema, M., Mori, D., Niwa, H., Hasegawa, Y., Yamanaka, Y., Hitoshi, S., Mimura, J., Kawabe, Y., Hosoya, T., Morita, M., et al. (2008). Krüppel-like factor 5 Is Essential for Blastocyst Development and the Normal Self-Renewal of Mouse ESCs. *Cell Stem Cell* 3, 555–567.

Ewels, P. A., Peltzer, A., Fillinger, S., Patel, H., Alneberg, J., Wilm, A., Garcia, M. U., Di Tommaso, P. and Nahnsen, S. (2020). The nf-core framework for community-curated bioinformatics pipelines. *Nature Biotechnology* 38, 276–278.

Faith, J. J., Hayete, B., Thaden, J. T., Mogno, I., Wierzbowski, J., Cottarel, G., Kasif, S., Collins, J. J. and Gardner, T. S. (2007). Large-Scale Mapping and Validation of Escherichia coli Transcriptional Regulation from a Compendium of Expression Profiles. *PLoS Biology* 5, e8.

Feizi, S., Marbach, D., Médard, M. and Kellis, M. (2013). Network deconvolution as a general method to distinguish direct dependencies in networks. *Nature Biotechnology* 31, 726–733.

Festuccia, N., Osorno, R., Halbritter, F., Karwacki-Neisius, V., Navarro, P., Colby, D., Wong, F., Yates, A., Tomlinson, S. R. and Chambers, I. (2012). Esrrb Is a Direct Nanog Target Gene that Can Substitute for Nanog Function in Pluripotent Cells. *Cell Stem Cell* 11, 477–490.

Fieller, E. C., Hartley, H. O. and Pearson, E. S. (1957). Tests for rank correlation coefficients. I. *Biometrika* 44, 470–481.

Fiers, M. W. E. J., Minnoye, L., Aibar, S., Bravo González-Blas, C., Kalender Atak, Z. and Aerts, S. (2018). Mapping gene regulatory networks from single-cell omics data. *Brief Funct Genomics* 17, 246–254.

Fleck, J. S., Jansen, S. M. J., Wollny, D., Zenk, F., Seimiya, M., Jain, A., Okamoto, R., Santel, M., He, Z., Camp, J. G., et al. (2022). Inferring and perturbing cell fate regulomes in human brain organoids. *Nature*.

Gerri, C., McCarthy, A., Alanis-Lobato, G., Demtschenko, A., Bruneau, A., Loubersac, S., Fogarty, N. M. E., Hampshire, D., Elder, K., Snell, P., et al. (2020). Initiation of a conserved trophectoderm program in human, cow and mouse embryos. *Nature* 587, 443–447.

González-Blas, C. B., De Winter, S., Hulselmans, G., Hecker, N., Matetovici, I., Christiaens, V., Poovathingal, S., Wouters, J., Aibar, S. and Aerts, S. (2022). SCENIC+: single-cell multiomic inference of enhancers and gene regulatory networks. *bioRxiv* 2022.08.19.504505.

Hainer, S. J., Bošković, A., McCannell, K. N., Rando, O. J. and Fazzio, T. G. (2019). Profiling of Pluripotency Factors in Single Cells and Early Embryos. *Cell* 177, 1319-1329.e11.

Haury, A.-C., Mordelet, F., Vera-Licona, P. and Vert, J.-P. (2012). TIGRESS: Trustful Inference of Gene REgulation using Stability Selection. *BMC Systems Biology* 6, 145.

Hayashi, R. and Inoue, A. (2023). Low-Input CUT&RUN for Mouse Oocytes and Preimplantation Embryos. *Methods Mol Biol* 2577, 83–92.

Hazimeh, H. and Mazumder, R. (2018). Fast Best Subset Selection: Coordinate Descent and Local Combinatorial Optimization Algorithms. *arXiv* arXiv:1803.01454,.

Huynh-Thu, V. A., Irrthum, A., Wehenkel, L. and Geurts, P. (2010). Inferring Regulatory Networks from Expression Data Using Tree-Based Methods. *PLoS ONE* 5, e12776.

Iacono, G., Massoni-Badosa, R. and Heyn, H. (2019). Single-cell transcriptomics unveils gene regulatory network plasticity. *Genome Biology* 20, 110.

Janssens, J., Aibar, S., Taskiran, I. I., Ismail, J. N., Gomez, A. E., Aughey, G., Spanier, K. I., De Rop, F. V., González-Blas, C. B., Dionne, M., et al. (2022). Decoding gene regulation in the fly brain. *Nature* 601, 630–636.

Kamimoto, K., Stringa, B., Hoffmann, C. M., Jindal K., Solnica-Krezel, L., and Morris, S. A. (2023). Dissecting cell identity via network inference and in silico gene perturbation. *Nature* 614, 742-751.

Kang, Y., Thieffry, D. and Cantini, L. (2021). Evaluating the Reproducibility of Single-Cell Gene Regulatory Network Inference Algorithms. *Front. Genet.* 12, 617282.

Kartha, V. K., Duarte, F. M., Hu, Y., Ma, S., Chew, J. G., Lareau, C. A., Earl, A., Burkett, Z. D., Kohlway, A. S., Lebofsky, R., et al. (2022). Functional inference of gene regulation using single-cell multi-omics. *Cell Genom* 2, 100166.

Kaya-Okur, H. S., Wu, S. J., Codomo, C. A., Pledger, E. S., Bryson, T. D., Henikoff, J. G., Ahmad, K. and Henikoff, S. (2019). CUT&Tag for efficient epigenomic profiling of small samples and single cells. *Nat Commun* 10, 1930.

Kim, J., T. Jakobsen, S., Natarajan, K. N. and Won, K.-J. (2021). TENET: gene network reconstruction using transfer entropy reveals key regulatory factors from single cell transcriptomic data. *Nucleic Acids Research* 49, e1–e1.

Krishnaswamy, S., Spitzer, M. H., Mingueneau, M., Bendall, S. C., Litvin, O., Stone, E., Pe'er, D. and Nolan, G. P. (2014). Conditional density-based analysis of T cell signaling in single-cell data. *Science* 346, 1250689.

Li, L., Guo, F., Gao, Y., Ren, Y., Yuan, P., Yan, L., Li, R., Lian, Y., Li, J., Hu, B., et al. (2018). Single-cell multi-omics sequencing of human early embryos. *Nature Cell Biology* 20,.

Li, Z., Schulz, M. H., Look, T., Begemann, M., Zenke, M. and Costa, I. G. (2019). Identification of transcription factor binding sites using ATAC-seq. *Genome Biology* 20,.

Lim, C. Y., Tam, W.-L., Zhang, J., Ang, H. S., Jia, H., Lipovich, L., Ng, H.-H., Wei, C.-L., Sung, W. K., Robson, P., et al. (2008). Sall4 Regulates Distinct Transcription Circuitries in Different Blastocyst-Derived Stem Cell Lineages. *Cell Stem Cell* 3, 543–554.

Lin, S.-C. J., Wani, M. A., Whitsett, J. A. and Wells, J. M. (2010). Klf5 regulates lineage formation in the pre-implantation mouse embryo. *Development* 137, 3953–3963.

Liu, L., Leng, L., Liu, C., Lu, C., Yuan, Y., Wu, L., Gong, F., Zhang, S., Wei, X., Wang, M., et al. (2019). An integrated chromatin accessibility and transcriptome landscape of human pre-implantation embryos. *Nature Communications* 10, 364.

Lv, B., An, Q., Zeng, Q., Zhang, X., Lu, P., Wang, Y., Zhu, X., Ji, Y., Fan, G. and Xue, Z. (2019). Single-cell RNA sequencing reveals regulatory mechanism for trophoblast cell-fate divergence in human peri-implantation conceptuses. *PLoS Biol* 17, e3000187.

960 Lyu, X., Rowley, M. J. and Corces, V. G. (2018). Architectural Proteins and Pluripotency Factors
961 Cooperate to Orchestrate the Transcriptional Response of hESCs to Temperature Stress.
962 *Molecular Cell* 71, 940-955.e7.
963 Marbach, D., Costello, J. C., Küffner, R., Vega, N. M., Prill, R. J., Camacho, D. M., Allison, K. R., The
964 DREAM5 Consortium, Kellis, M., Collins, J. J., et al. (2012). Wisdom of crowds for robust gene
965 network inference. *Nature Methods* 9, 796–804.
966 Margolin, A. A., Nemenman, I., Basso, K., Wiggins, C., Stolovitzky, G., Favera, R. D. and Califano, A.
967 (2006). ARACNE: An Algorithm for the Reconstruction of Gene Regulatory Networks in a
968 Mammalian Cellular Context. *BMC Bioinformatics* 7, S7.
969 Materna, S. C. and Davidson, E. H. (2007). Logic of gene regulatory networks. *Curr Opin Biotechnol.* 4,
970 351–354.
971 Meers, M. P., Bryson, T. D., Henikoff, J. G. and Henikoff, S. (2019). Improved CUT&RUN chromatin
972 profiling tools. *eLife* 8,.
973 Meistermann, D., Bruneau, A., Loubersac, S., Reignier, A., Firmin, J., François-Campion, V., Kilens, S.,
974 Lelièvre, Y., Lammers, J., Feyeux, M., et al. (2021). Integrated pseudotime analysis of human
975 pre-implantation embryo single-cell transcriptomes reveals the dynamics of lineage
976 specification. *Cell Stem Cell* 28, 1625-1640.e6.
977 Mitsui, K., Tokuzawa, Y., Itoh, H., Segawa, K., Murakami, M., Takahashi, K., Maruyama, M., Maeda,
978 M. and Yamanaka, S. (2003). The homeoprotein Nanog is required for maintenance of
979 pluripotency in mouse epiblast and ES cells. *Cell* 113, 631–642.
980 Mochida, K., Koda, S., Inoue, K. and Nishii, R. (2018). Statistical and Machine Learning Approaches to
981 Predict Gene Regulatory Networks From Transcriptome Datasets. *Front Plant Sci* 9, 1770.
982 Morris, S. A., Cahan, P., Li, H., Zhao, A. M., San Roman, A. K., Shivdasani, R. A., Collins, J. J. and Daley,
983 G. Q. (2014). Dissecting engineered cell types and enhancing cell fate conversion via CellNet.
984 *Cell* 158, 889–902.
985 Nguyen, H., Tran, D., Tran, B., Pehlivan, B. and Nguyen, T. (2021). A comprehensive survey of
986 regulatory network inference methods using single cell RNA sequencing data. *Briefings in*
987 *Bioinformatics* 22, bbaa190.
988 Niakan, K.K. and Eggan K. (2012). Analysis of human embryos from zygote to blastocyst reveals
989 distinct gene expression patterns relative to the mouse. *Developmental Biology* 375, 54-64.
990
991 Niakan, K. K., Han, J., Pedersen, R. A., Simon, C. and Pera, R. A. R. (2012). Human pre-implantation
992 embryo development. *Development* 139, 829–841.
993 Pastor, W. A., Liu, W., Chen, D., Ho, J., Kim, R., Hunt, T. J., Lukianchikov, A., Liu, X., Polo, J. M.,
994 Jacobsen, S. E., et al. (2018). TFAP2C regulates transcription in human naive pluripotency by
995 opening enhancers. *Nat Cell Biol* 20, 553–564.
996 Pe'er, D. (2005). Bayesian Network Analysis of Signaling Networks: A Primer. *Science Signaling* 2005,
997 pl4–pl4.
998 Peter, I. S. and Davidson, E. H. (2011). Evolution of Gene Regulatory Networks Controlling Body Plan
999 Development. *Cell* 144, 970–985.
1000 Petropoulos, S., Edsgärd, D., Reinius, B., Deng, Q., Panula, S. P., Codeluppi, S., Plaza Reyes, A.,
1001 Linnarsson, S., Sandberg, R. and Lanner, F. (2016). Single-Cell RNA-Seq Reveals Lineage and X
1002 Chromosome Dynamics in Human Preimplantation Embryos. *Cell* 165, 1012–1026.
1003 Picelli, S., Faridani, O. R., Björklund, A. K., Winberg, G., Sagasser, S. and Sandberg, R. (2014). Full-
1004 length RNA-seq from single cells using Smart-seq2. *Nat Protoc* 9, 171–181.
1005 Pratapa, A., Jalihal, A. P., Law, J. N., Bharadwaj, A. and Murali, T. M. (2020). Benchmarking
1006 algorithms for gene regulatory network inference from single-cell transcriptomic data.
1007 *Nature Methods* 17, 147–154.
1008 Roode, M., Blair K., Snell, P., Elder, K., Marchant, S., Smith, A., Nichols, J. (2012). Human hypoblast
1009 formation is not dependent on FGF signalling. *Developmental Biology* 361, 358-363.
1010

1011 Schneider, C. A., Rasband, W. S. and Eliceiri, K. W. (2012). NIH Image to ImageJ: 25 years of image
1012 analysis. *Nat Methods* 9, 671–675.
1013 Schoenfelder, S. and Fraser, P. (2019). Long-range enhancer-promoter contacts in gene expression
1014 control. *Nat Rev Genet* 20, 437–455.
1015 Shi, W., Wang, H., Pan, G., Geng, Y., Guo, Y. and Pei, D. (2006). Regulation of the Pluripotency
1016 Marker Rex-1 by Nanog and Sox2. *Journal of Biological Chemistry* 281, 23319–23325.
1017 Shu, H., Zhou, J., Lian, Q., Li, H., Zhao, D., Zeng, J. and Ma, J. (2021). Modeling gene regulatory
1018 networks using neural network architectures. *Nature Computational Science* 1, 491–501.
1019 Skene, P. J. and Henikoff, S. (2017). An efficient targeted nuclease strategy for high-resolution
1020 mapping of DNA binding sites. *eLife* 6, e21856.
1021 Stirling, D. R., Swain-Bowden, M. J., Lucas, A. M., Carpenter, A. E., Cimini, B. A. and Goodman, A.
1022 (2021). CellProfiler 4: improvements in speed, utility and usability. *BMC Bioinformatics* 22,
1023 433.
1024 Stone, M., Li, J., McCalla, S. G., Siahpirani, A. F., Periyasamy, V., Shin, J. and Roy, S. (2021). Identifying
1025 strengths and weaknesses of methods for computational network inference from single cell
1026 RNA-seq data. *bioRxiv* 2021.06.01.446671,.
1027 Strumpf, D., Mao, C.-A., Yamanaka, Y., Ralston, A., Chawengsaksophak, K., Beck, F. and Rossant, J.
1028 (2005). Cdx2 is required for correct cell fate specification and differentiation of
1029 trophectoderm in the mouse blastocyst. *Development* 132, 2093–2102.
1030 Thompson, D., Regev, A. and Roy, S. (2015). Comparative analysis of gene regulatory networks: from
1031 network reconstruction to evolution. *Annu Rev Cell Dev Biol* 31, 399–428.
1032 Tibshirani, R. (1996). Regression Shrinkage and Selection Via the Lasso. *Journal of the Royal*
1033 *Statistical Society: Series B (Methodological)* 58, 267–268.
1034 Tipping, M. E. (2001). Sparse Bayesian Learning and the Relevance Vector Machine. *Journal of*
1035 *Machine Learning Research* 1, 211–244.
1036 Wang, B., Pourshafeie, A., Zitnik, M., Zhu, J., Bustamante, C. D., Batzoglou, S. and Leskovec, J. (2018).
1037 Network enhancement as a general method to denoise weighted biological networks.
1038 *Nature Communications* 9,.
1039 Wang, J., Ma, A., Ma, Q., Xu, D. and Joshi, T. (2020). Inductive inference of gene regulatory network
1040 using supervised and semi-supervised graph neural networks. *Computational and Structural*
1041 *Biotechnology Journal* 18, 3335–3343.
1042 Wang, X., He, Y., Zhang, Q., Ren, X. and Zhang, Z. (2021). Direct Comparative Analyses of 10X
1043 Genomics Chromium and Smart-seq2. *Genomics Proteomics Bioinformatics* 19, 253–266.
1044 Weigert, M., Schmidt, U., Haase, R., Sugawara, K. and Myers, G. (2020). Star-convex Polyhedra for 3D
1045 Object Detection and Segmentation in Microscopy. In *2020 IEEE Winter Conference on*
1046 *Applications of Computer Vision (WACV)*, pp. 3655–3662. Snowmass Village, CO, USA: IEEE.
1047 Yan, L., Yang, M., Guo, H., Yang, L., Wu, J., Li, R., Liu, P., Lian, Y., Zheng, X., Yan, J., et al. (2013).
1048 Single-cell RNA-Seq profiling of human preimplantation embryos and embryonic stem cells.
1049 *Nature Structural & Molecular Biology* 20, 1131–1139.
1050 Zheng, G. X. Y., Terry, J. M., Belgrader, P., Ryvkin, P., Bent, Z. W., Wilson, R., Ziraldo, S. B., Wheeler, T.
1051 D., McDermott, G. P., Zhu, J., et al. (2017). Massively parallel digital transcriptional profiling
1052 of single cells. *Nat Commun* 8, 14049.
1053 Zou, H. and Hastie, T. (2005). Regularization and variable selection via the elastic net. *J Royal*
1054 *Statistical Soc B* 67, 301–320.
1055
1056
1057
1058
1059
1060 **Figure legends**
1061

Figure 1. An overview of the regulatory network inference, evaluation, and validation framework and inference on simulated scRNA-seq data. (A) Footprinting analysis was applied to ATAC-seq data from human embryos at the late blastocyst stage to identify potential transcription factor (TF) binding sites and TF-gene regulations. The TFs and genes in this list of chromatin accessibility (CA)-predicted regulations were used to refine the size of scRNA-seq data from each of the cell types in embryos where cells were collected at the same developmental stage (EPI: Epiblast, 26 cells; PE: Primitive Endoderm, 33 cells; TE: Trophectoderm, 45 cells). Four gene regulatory network (GRN) inference approaches and a random approach were applied to the scRNA-seq data. The scRNA-seq data were normalised using four different methods for comparison (log(TPM+1), log(FPKM+1), batch-corrected and log-counts).The reproducibility and biological context of the predicted GRNs were evaluated using several statistical tests. GRNs refined by keeping CA-predicted regulations only were also evaluated. Squares represent genes that regulate other genes, and circles represent genes that are regulated by other genes. **(B)** Comparison of different GRN inference methods (L0L2, GENIE3, Spearman correlation and MI) to recover the ground-truth GRN structure from simulated gene expression data as measured with the average area under the receiver operating characteristic curve (AUROC) from 100 simulations. The average AUROC is shown as a function of different sample sizes (n=10 to 1000) and the number of potential regulators of each gene in the simulated datasets is also varied from 10 to 100. The range of sizes of the three human blastocyst datasets that we analysed is highlighted in grey as a reference. Error bars correspond to standard errors of the mean. **(C)** Box-and-whisker plots show comparison of AUROC values for all simulations for each method with number of samples n=100 and number of regulators p=20, 50 and 100.

Figure 2. Statistical comparison of four different methods to infer early human embryo GRNs. Robustness of the GRNs predicted by four inference methods with or without chromatin accessibility (CA) refinement was evaluated by three different metrics. **(A)** ΔR measures the difference between the median edge-level reproducibility for a GRN inference method and a random predictor. **(B)** ΔAUPRC quantifies the extent to which the interactions inferred from half of a dataset coincide with the top-1% interactions inferred from the second half. This 2-fold cross-validation experiment was repeated ten times and compared to a random predictor. **(C)** The inverse of the normalised L2 loss between the network scores from the two folds was computed. L0L2 did not converge when applied to the TE dataset. All data used was generated using the SMART-seq2 sequencing technique.

Figure 3. Evaluation of the biological relevance of inferred GRNs in the context of early human development. (A) Two-dimensional UMAP representation of the scRNA-seq data from each of the three cell types in the early human at the blastocyst stage. The expression of marker genes for each cell type is also represented in UMAP space: NANOG is used as an Epiblast marker, CDX2 as a Trophectoderm marker and GATA4 as a Primitive endoderm marker. **(B)** Marker activity in the cell-type specific GRNs (EPI: Epiblast, PE: Primitive endoderm; TE: Trophectoderm) and the network common to the three cell types in the human blastocyst. The expected pattern, i.e. the marker that was expected to be active in each GRN, is shown for reference. **(C)** Normalised V-statistic across datasets and inference methods. V corresponds to the number of gene sets that were enriched at a significance level of 10% in a gene set enrichment analysis performed with the genes involved in the top-500 regulations by the 25 most-connected TFs in the EPI or TE GRNs. All sequencing was performed using the SMART-seq2 technique.

Figure 4. TF GRNs predicted by MICA to be regulated by, or to regulate, NANOG, GATA4 or CDX2. Target networks contain a maximum of 25 potential target TFs of the hub (or central) TF, whereas regulator networks include a maximum of 25 TFs that potentially regulate the hub. The average expression of the transcript is represented by the size of the TF node. MI scores are represented by the thickness of the line in the predicted network. To further refine the MICA-predictions we used the Spearman's rank correlation coefficient between the

expression levels of the source and target nodes to define correlated or anti-correlated expression. Correlated or anti-correlated node pairs correspond to positive or negative Spearman's rank coefficient with p-value smaller than 0.1. Node pairs with a p-value equal to or larger than 0.1 were defined as uncorrelated, though they are predicted by MICA. **(A)** Network of TFs predicted to be targeted by NANOG. **(B)** Network of TFs that are predicted to regulate NANOG. **(C)** Network of TFs predicted to be targeted by GATA4. **(D)** Network of TFs that that are predicted to regulate GATA4. **(E)** Network TFs predicted to be targeted by CDX2. **(F)** Network of TFs that are predicted to regulate CDX2.

Figure 5. MICA predicted conserved TFAP2C interactions in human early embryo EPI, TE, and PE cells. (A) Network composed of TFAP2C, JUND, SOX4, and GCM1 in EPI (left), TE (middle), and PE (right). **(B)** Correlation plots between TFAP2C, JUND, SOX4, and GCM1 in TE cells. Bottom left: log transformed RNA expression of genes in single cells. Diagonal: Distribution of log transformed RNA expression for TFAP2C, JUND, SOX4 and GCM1. Top right: Spearman correlation between TF pairs. (***: $p < 0.001$). **(C)** Immunofluorescence staining of TFAP2C and JUND in E6.5 human blastocysts. **(D)** Correlation plot of TFAP2C and JUND protein expression intensity in nuclei of human E6.5 blastocysts. Numbers on the plot are Pearson correlation value. (***: $p < 0.001$).

1138 **Figure 1**

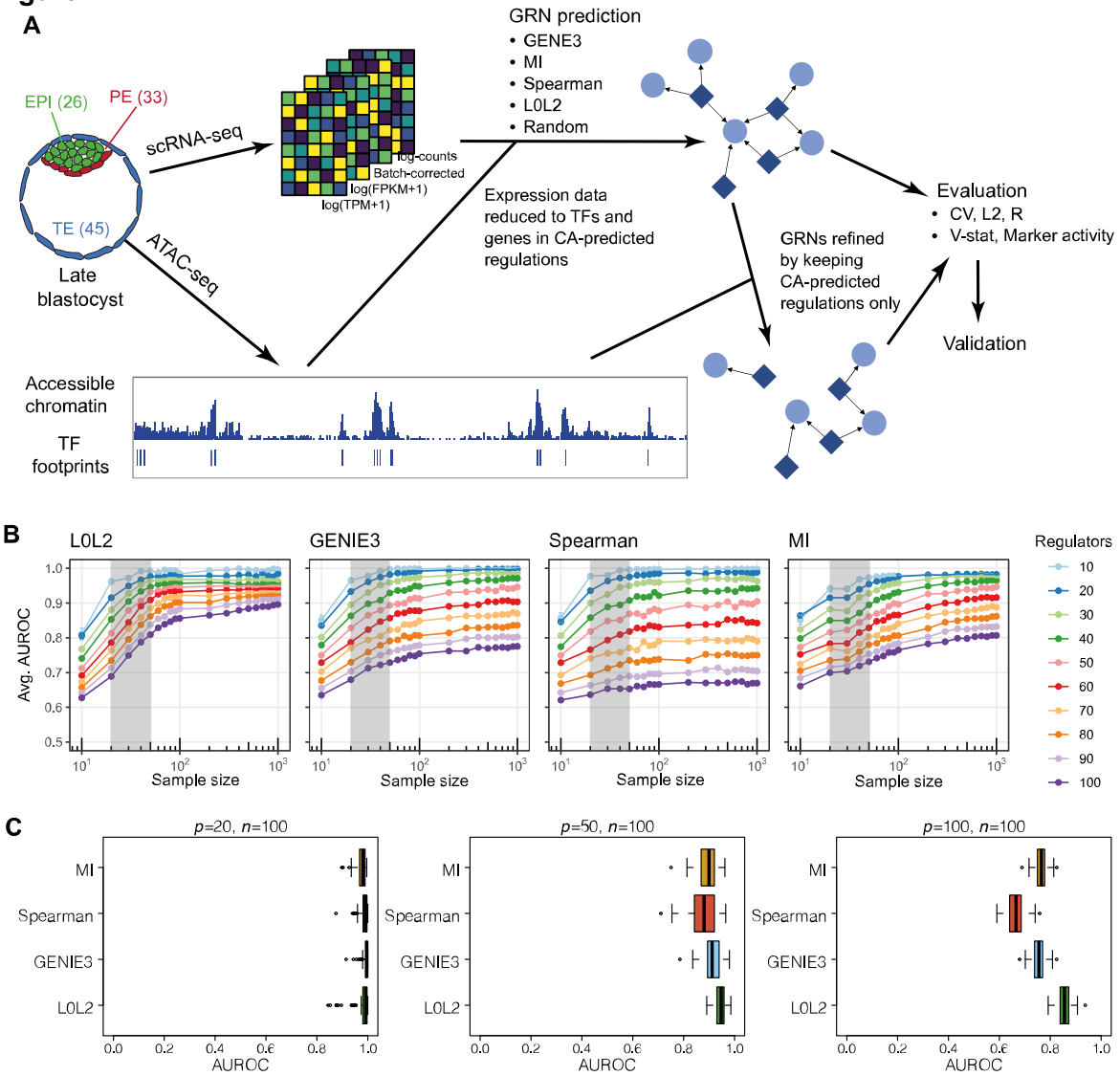

1139

Figure 2

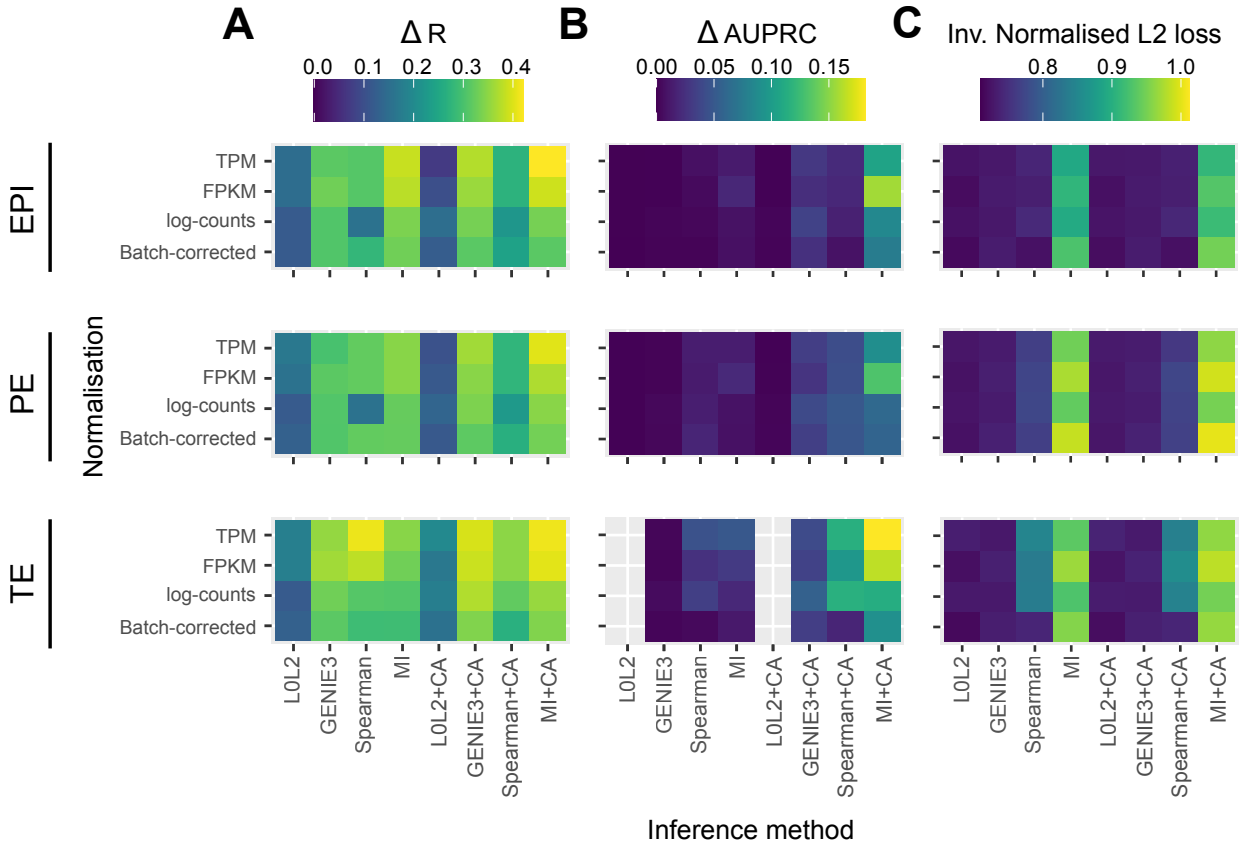
A
Δ R
0.0 0.1 0.2 0.3 0.4
B
Δ AUPRC
0.00 0.05 0.10 0.15
C
Inv. Normalised L2 loss
0.8 0.9 1.0
EPI
PE
TE
Normalisation
TPM
FPKM
log-counts
Batch-corrected
L0L2
GENIE3
Spearman
MI
L0L2+CA
GENIE3+CA
Spearman+CA
MI+CA
Inference method

1143 **Figure 3**
1144

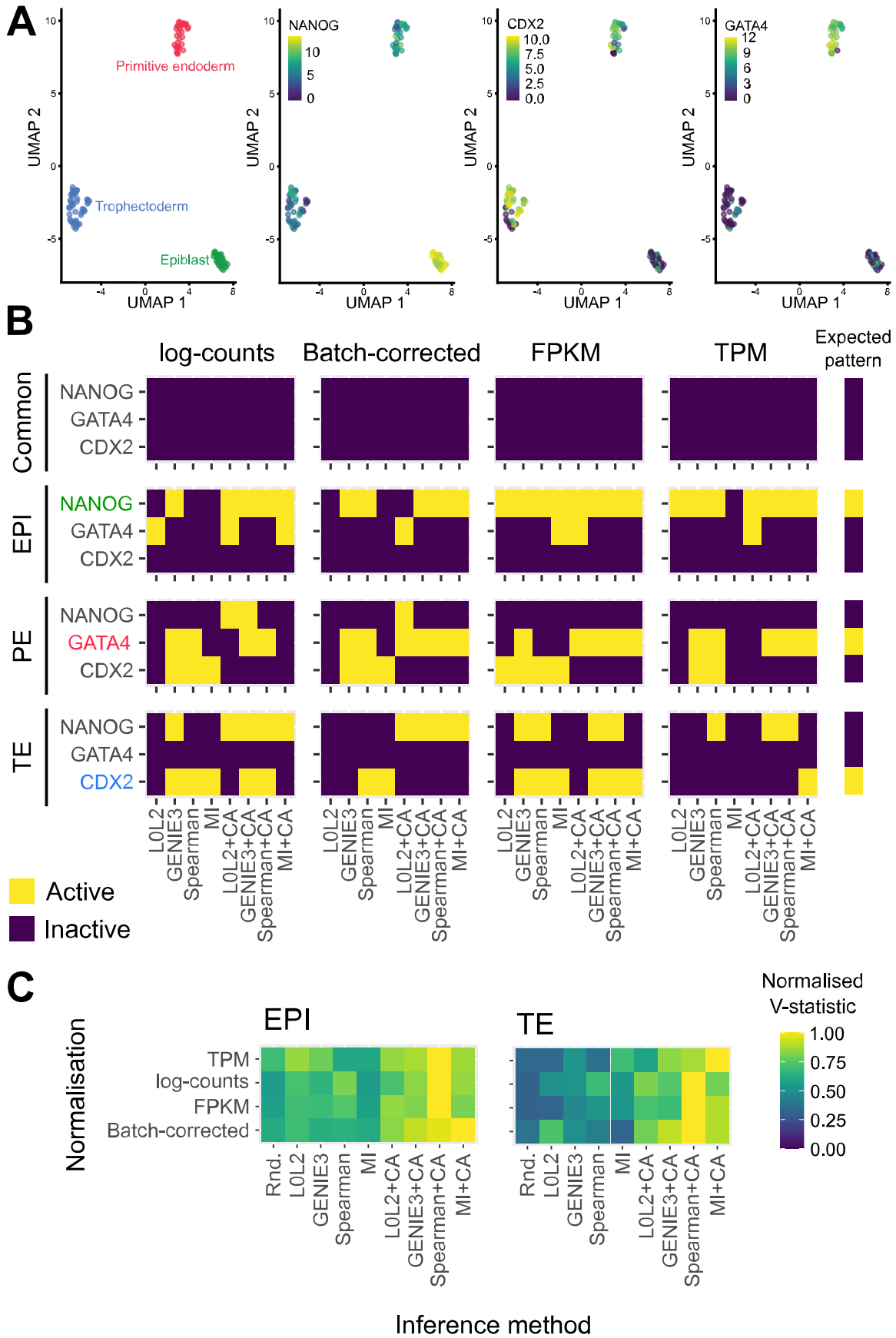

1145

Figure 4

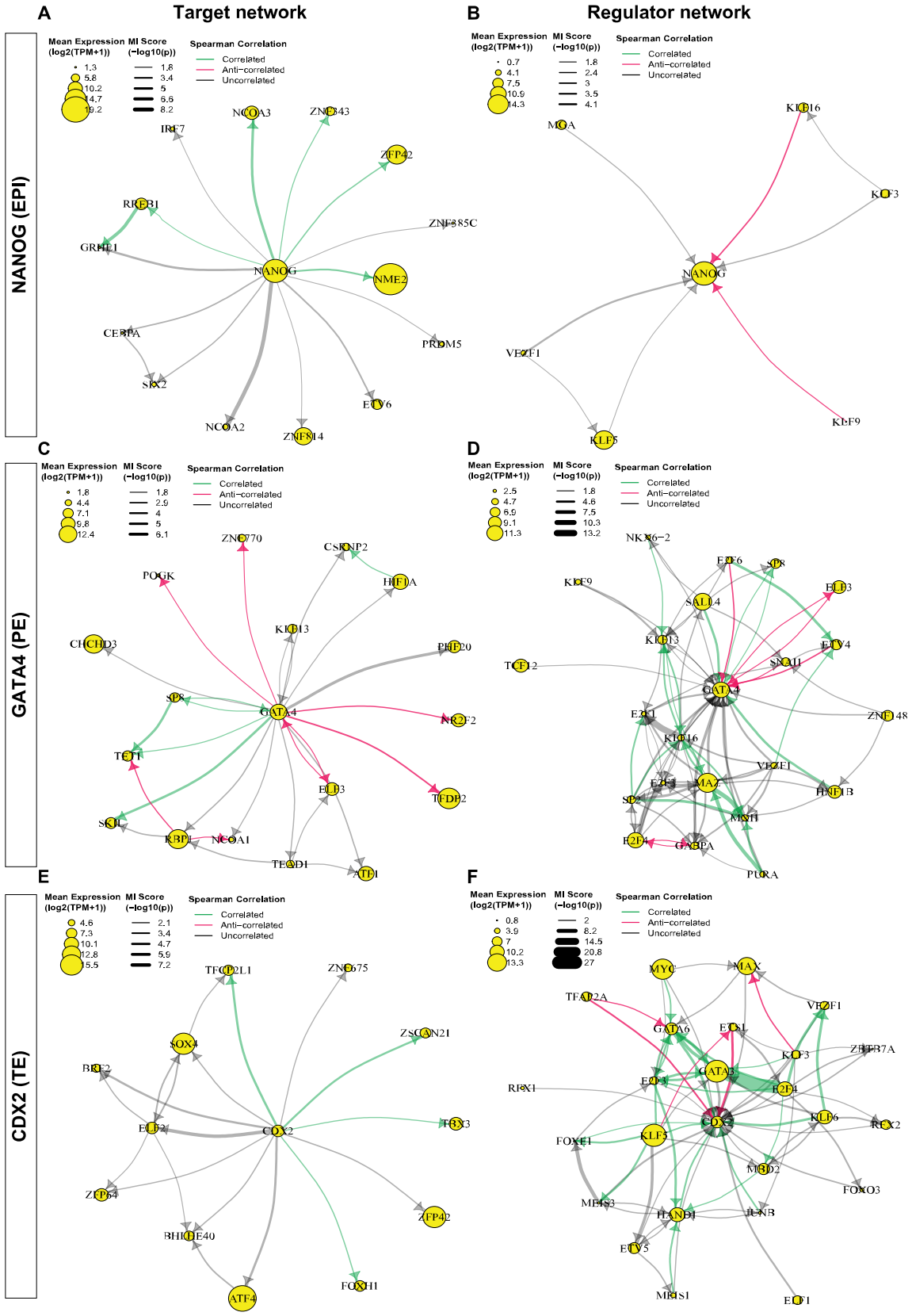
A
Target network
B
Regulator network
NANOG (EPI)
GATA4 (PE)
CDX2 (TE)
C
D
E
F
Mean Expression (log2(TPM+1))
MI Score (−log10(p))
Spearman Correlation
Correlated
Anti−correlated
Uncorrelated
NANOG
NME2
ZFP42
ZNF385C
PROM5
ETV6
ZNF814
NCOA2
SKX2
CEBPA
GRHL1
RREB1
IRF7
NCOA3
ZNF343
MGA
KLF16
KLF3
KLF9
KLF5
VEZF1
GATA4
ZNF770
CSKNP2
HIF1A
POGK
KLF13
CHCHD3
PHF20
SP8
NR2F2
TET1
ELF3
TFDP2
SKIL
RBPJ
NCOA1
TEAD1
ATF1
NKX6−2
E2F6
SP8
ELF3
KLF9
SALL4
KLF13
ETV4
TCF12
SNAI1
GATA4
ZNF148
E2F1
KLF16
VEZF1
E2F3
MAZ
HNF1B
SP2
MXI1
E2F4
GABPA
PURA
TFCP2L1
ZNF675
ZSCAN21
SOX4
BRF2
ELF2
CDX2
TBX3
ZFP64
ZFP42
BHLHE40
ATF4
FOXH1
MYC
MAX
TFAP2A
VEZF1
GATA6
ETS1
KLF3
ZBTB7A
GATA3
RFX1
E2F3
E2F4
CDX2
KLF6
RFX2
FOXE1
KLF5
MBD2
FOXO3
MEIS3
HAND1
JUNB
ETV5
MEIS1
ELF1

Figure 5

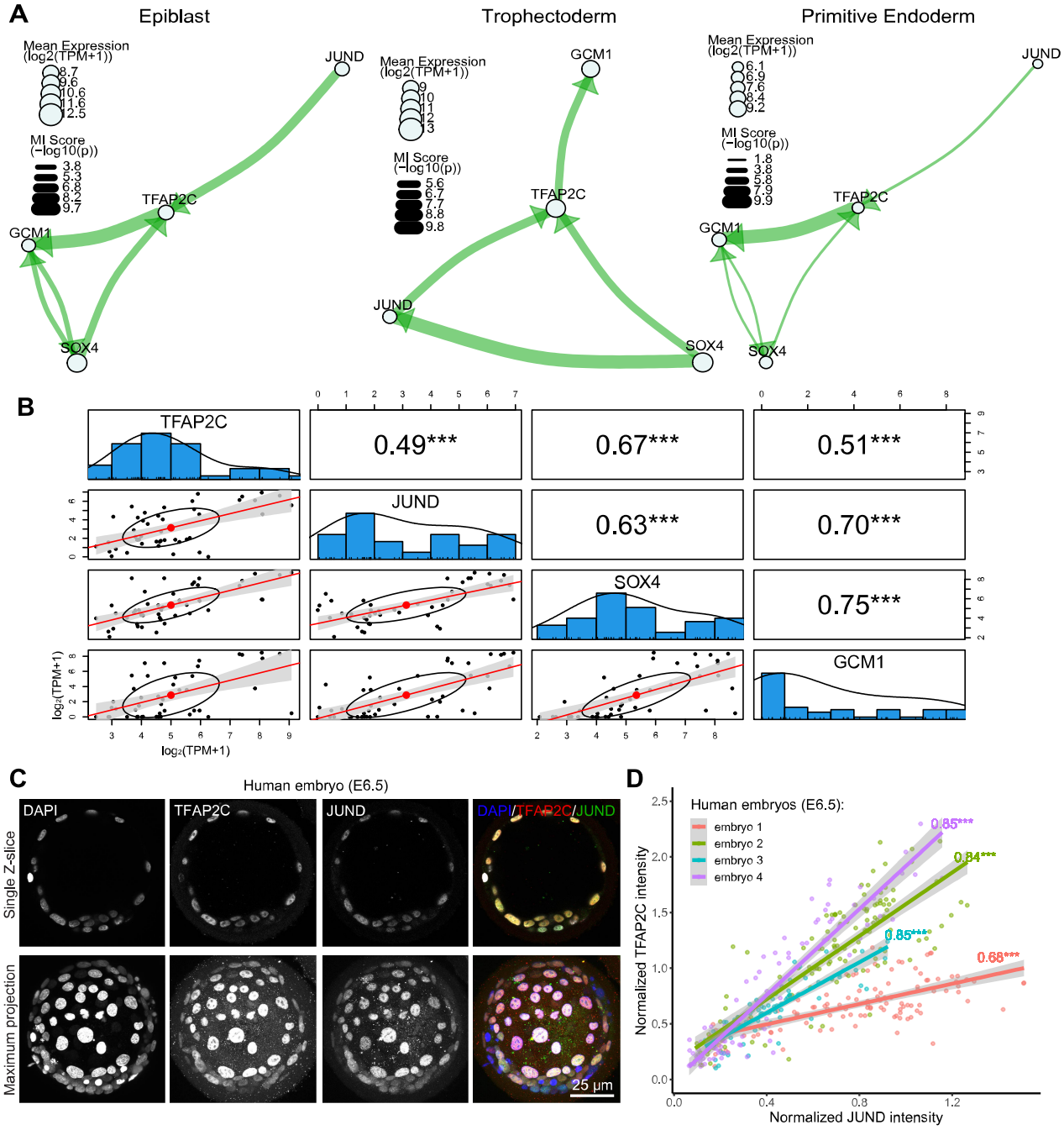
A
Epiblast
Trophectoderm
Primitive Endoderm
Mean Expression (log2(TPM+1))
MI Score (−log10(p))
GCM1
TFAP2C
JUND
SOX4
B
TFAP2C
JUND
SOX4
GCM1
0.49***
0.67***
0.51***
0.63***
0.70***
0.75***
log2(TPM+1)
C
Human embryo (E6.5)
DAPI
TFAP2C
JUND
DAPI/TFAP2C/JUND
Single Z-slice
Maximum projection
25 µm
D
Human embryos (E6.5):
embryo 1
embryo 2
embryo 3
embryo 4
0.85***
0.84***
0.85***
0.68***
Normalized TFAP2C intensity
Normalized JUND intensity